Moscoso, M., Novikov, A., Papanicolaou, G. & Tsogka, C. (2020). Synthetic Aperture Imaging With Intensity-Only Data. *IEEE Transactions on Computational Imaging*, 6, pp. 87–94.

DOI: 10.1109/TCI.2019.2919272

Synthetic aperture imaging with intensity-only measurements

Miguel Moscoso[1], Alexei Novikov[2], George Papanicolaou[3], and Chrysoula Tsogka[4]
[1]Department of Mathematics, Universidad Carlos III de Madrid, Leganes, Madrid 28911, Spain
[2]Mathematics Department, Penn State University, University Park, PA 16802
[3]Department of Mathematics, Stanford University, Stanford, CA 94305
[4]Applied Math Unit, University of California, Merced, 5200 North Lake Road, Merced, CA 95343

We consider imaging the reflectivity of scatterers from intensity-only data recorded by a single moving transducer that both emits and receives signals, forming a synthetic aperture. By exploiting frequency illumination diversity we obtain multiple measurements for each location from which we determine missing phase information using an appropriate illumination strategy and the polarization identity. The phase cross-correlations obtained this way from intensities do not, however, provide all the missing information. The main result of this paper is an algorithm with which we can recover all the missing phases up to a single unknown global phase. We can therefore image coherently over all frequencies and measurement locations as if full phase information was recorded.

I. Introduction

Synthetic aperture imaging when only intensities of signals are recorded is a challenge because imaging algorithms rely in an essential way on the missing phase information. There is considerable recent interest in methods that attempt to recover the missing phase information (see [9] and references therein) driven by a variety of applications. This is mainly because there is a need for more compact, inexpensive, and robust imaging systems. One important application is in security screening systems where both cost and time for data acquisition are reduced when intensity only detectors are employed. Robustness with intensity-only imaging systems is likely to be enhanced because probe position errors due to positioning and misalignment can be reduced.

One frequently used method to recover the missing phase information is to collect intensity data at two parallel surfaces, and propagate the fields iteratively from one surface to another to find the missing phases with Fienup's Hybrid-Input-Output algorithm [8], [7]. It works well on well-separated planes, but if the separation is small convergence to local minima may occur. Convergence may be achieved, however, by using global optimization methods which are time consuming [17].

Several non-iterative or direct methods have also been developed to avoid convergence issues. These are interferometric approaches that rely on recovering phase field differences from intensity data. In [12], the authors use the responses to two probe antennas recorded at three intensity-only or power detectors to obtain antenna phase patterns. In [6], a similar approach is used along with a minimization procedure that finds the missing phases. Despite the nonlinearity of the problem, the authors report an accurate and fast convergence of their method, without stagnation problems. A holographic technique that combines a known reference signal with the received signals is also used in [11] for characterization of complex antenna patterns. However, it cannot be used in a monostatic setup because it requires a transformation from the spatial to the spectral domain that is only possible if measurements can be recorded simultaneously at several locations. Recently, a modified holography technique for monostatic multifrequency scanning antennas has been proposed in [9], [10]. In this case, a transformation from the time domain to the frequency domain is used.

Manuscript received August 31, 2018; Corresponding author: C. Tsogka(email: ctsogka@ucmerced.edu)

In this paper, we present a new approach to accurately reconstruct the reflectivity of scatterers with synthetic aperture, intensity-only data. The method has two stages. First, we obtain for each receiver location phase cross-correlations from the recorded intensities. This is done using a special sequence of illuminations and the polarization identity as in [16], [14]. From these cross-correlations we recover the missing phases up to a phase that depends on the receiver location. In the second stage we introduce a new algorithm that recovers these location dependent phases, and this is the main result of this paper. With this approach, we show that imaging with intensity-only data can be as good as imaging with full data.

The paper is organized as follows. In Section II, we explain the proposed method to obtain coherent cross-correlations when only one element that measures only intensities is used for both receiving and transmitting purposes. In Section III, we discuss two imaging methods usually used with full phase and amplitude data that can be used with the recovered cross-correlations. In Section IV, we show the results of our numerical experiments. Section V contains our conclusions.

II. Multi-frequency interferometric synthetic aperture imaging

In the next two subsections we present in detail the two stages of the proposed approach for recovering the missing phases from intensity only synthetic aperture data.

A. Multi-frequency cross-corellations

Let $|P(x_j,\omega_l)|$ be the amplitude of the signal received at location $\boldsymbol{x}_j$ when a signal of unit amplitude and zero phase is emitted from the same location at frequency ω_l. The goal is to determine the reflectivity ρ within a region of interest, called the image window IW, from multiple measurements at different locations $\boldsymbol{x}_j$, $j=1,\ldots,N$, and frequencies ω_l, $l=$

$1, \ldots, S$ (see Figure 1), with a total number of $D = N \cdot S$ data. For imaging purposes, the IW is discretized using a uniform grid of K points $\boldsymbol{y}_k$, $k = 1, \ldots, K$. The unknown is the *reflectivity vector* $\boldsymbol{\rho} = [\rho_1, \ldots, \rho_K]^t \in \mathbb{C}^K$, whose entries are the values of the reflectivity $\rho_k = \rho(\boldsymbol{y}_k)$ on the grid points $\boldsymbol{y}_k$, $k = 1, \ldots, K$. We assume that $K > D$, and often we have $K \gg D$.

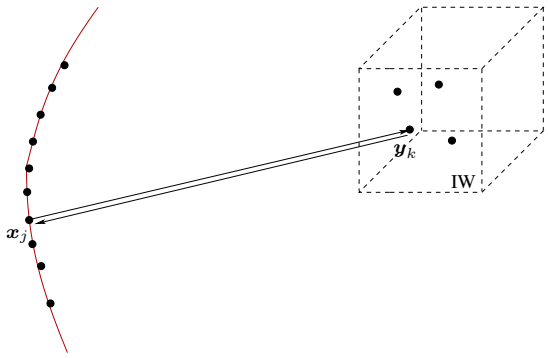

Fig. 1. General setup of a synthetic aperture imaging problem. The transducer at $\boldsymbol{x}_j$ emits a probing signal and the reflected intensities are recorded at the same location for all illuminations. The scatterers are located inside the image window IW which is discretized with the grid points $\boldsymbol{y}_k$, $k = 1, \ldots, K$.

We pursue here the idea of [16], [14], [15], where it is shown that cross-correlations can be obtained from intensity-only measurements by using an appropriate protocol of illuminations and the polarization identity. However, because in synthetic aperture imaging a single transmitter/receiver element is used, there is an inherent loss of flexibility in the illumination strategy compared to array imaging applications in which all the elements of the array are used to emit and receive signals. This lack of flexibility in illuminations might suggest that the collected data cannot be used coherently to form images in synthetic aperture imaging if only intensities are measured.

To explain this further, we introduce the following row vector $\mathbf{P}^j \in \mathbb{C}^S$ with components $P(x_j, \omega_l)$ corresponding to the signal recorded at $\boldsymbol{x}_j$, including phases, when a unit amplitude and zero phase signal is send from the same location

$$\mathbf{P}^j = [P(\boldsymbol{x}_j, \omega_1) \quad P(\boldsymbol{x}_j, \omega_2) \quad \ldots \quad P(\boldsymbol{x}_j, \omega_S)] \ . \tag{1}$$

The first step of the proposed methodology consists in recovering, at every fixed location $\boldsymbol{x}_j$, the cross-correlation matrix

$$[\boldsymbol{M}^j]_{ll'} \equiv m^j_{ll'} = \overline{P(\boldsymbol{x}_j, \omega_l)} P(\boldsymbol{x}_j, \omega_{l'}), \quad l, l' = 1, \ldots, S \ . \tag{2}$$

To do so we use diversity over frequencies of illuminations and the polarization identities

$$\mathrm{Re}(m^j_{ll'}) = \frac{1}{2}\left(|\mathbf{P}^j \cdot \boldsymbol{e}_{l+\imath l'}|^2 - |\mathbf{P}^j \cdot \boldsymbol{e}_l|^2 - |\mathbf{P}^j \cdot \boldsymbol{e}_{l'}|^2\right) \tag{3}$$

$$\mathrm{Im}(m^j_{ll'}) = \frac{1}{2}\left(|\mathbf{P}^j \cdot \boldsymbol{e}_{l-\imath l'}|^2 - |\mathbf{P}^j \cdot \boldsymbol{e}_l|^2 - |\mathbf{P}^j \boldsymbol{e}_{l'}|^2\right). \tag{4}$$

Here $\boldsymbol{e}_l \in \mathbb{C}^S$ is the vector with a 1 in the l-th coordinate and 0's elsewhere. It represents a signal of unit amplitude and phase zero at frequency ω_l. In (3)-(4), $\imath = \sqrt{-1}$, $\boldsymbol{e}_{l+l'} = \boldsymbol{e}_l + \boldsymbol{e}_{l'}$, and $\boldsymbol{e}_{l-\imath l'} = \boldsymbol{e}_l - \imath \boldsymbol{e}_{l'}$. Note that the vector $\boldsymbol{e}_{l+l'} = \boldsymbol{e}_l + \boldsymbol{e}_{l'}$ refers to sending simultaneously signals of unit amplitude and phase zero at two frequencies, ω_l and $\omega_{l'}$, while the vector $-\imath \boldsymbol{e}_{l'}$ denotes a π rad frequency domain shifting of the signal corresponding to frequency $\omega_{l'}$. Since all entries on the right-hand side in these equations involve quadratic quantities, we can recover all the entries in $\boldsymbol{M}^j$ even when phases are not recorded. We propose in Appendix A an illumination strategy that requires measurements corresponding to $3S-2$ illuminations so as to recover all the entries in $\boldsymbol{M}^j$. This illumination strategy can be used when either intensities are recorded or total power is the only measured quantity. Typically the total power is much easier to obtain.

Note, however, that $\boldsymbol{M}^j$ is recovered up to an unknown global phase that depends on each receiver location $\boldsymbol{x}_j$. These phases, which are independent of frequency, are needed in order to superpose images coherently over the antenna locations. This is the main difficulty in synthetic aperture imaging when the phases are not measured. We explain how to overcome this problem next.

B. Missing location-dependent phase recovery

As described previously, we can recover, up to a global phase that depends on the receiver location $\boldsymbol{x}_j$, cross-correlations of the form (2) using frequency diversity in the illuminations and the polarization identities. Note that $|P(\boldsymbol{x}_j, \omega_l)|$ is also known for $l = 1, \ldots, S$ at every location $\boldsymbol{x}_j$, since intensities are recorded. Therefore given the correlation matrix elements $m^j_{ll'}$, $l, l' = 1, \ldots, S$, as in (2), we can compute up to a global phase

$$\frac{m^j_{ll'}}{|P(\boldsymbol{x}_j, \omega_l)|} = P(\boldsymbol{x}_j, \omega_{l'}) \frac{\overline{P(\boldsymbol{x}_j, \omega_l)}}{|P(\boldsymbol{x}_j, \omega_l)|}, \ l' = 1, \ldots, S,$$

which means that the typical data can be recovered at each measurement location $\boldsymbol{x}_j$ up to a global phase θ_j which is unknown,

$$P(\boldsymbol{x}_j, \omega_l) e^{\imath \theta_j}, \ \text{for } l = 1, \ldots, S. \tag{5}$$

To image coherently, we are going to refer all these unknown phases to a single location.

By linearizing the scattering problem, and assuming a homogeneous background with velocity c, the data is given by

$$P(\boldsymbol{x}_j, \omega_l) = \sum_{q=1}^{Q} \tilde{\rho}_q e^{\imath 2 \frac{\omega_l}{c} r^j_q}, \tag{6}$$

where $\tilde{\rho}_q$ is the integral of the reflectivity on the sphere of radius r^j_q centered at $\boldsymbol{x}_j$; see Figure 2. It follows from (6) that the data $P(\boldsymbol{x}_j, \omega_l)$ is the Fourier coefficient of the reflectivity $\tilde{\rho}$ corresponding to wavenumber $\kappa_l = 2\frac{\omega_l}{c}$,

$$\widehat{\tilde{\rho}}(\kappa_l) = \sum_{q=1}^{Q} \tilde{\rho}_q e^{\imath \kappa_l r^j_q}.$$

Therefore at each source-detector position we have to solve a phase retrieval problem for one dimensional Fourier data. The

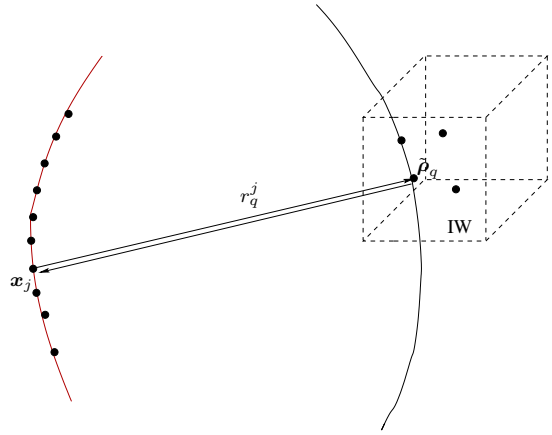

Fig. 2. The data (with phases) $P(\boldsymbol{x}_j, \omega_l)$ recorded at transducer $\boldsymbol{x}_j$ when a unit amplitude signal with phase zero at frequency ω_l is emitted from the same location is given by the model (6) where $\tilde{\rho}_q$ is the integral of the unknown reflectivity on the sphere centered at $\boldsymbol{x}_j$ of radius r_q^j.

unknown vector $\tilde{\boldsymbol{\rho}} = [\tilde{\rho}_1, \tilde{\rho}_2, \ldots, \tilde{\rho}_Q]$ can be determined by solving a linear system

$$\mathcal{A}^j \tilde{\boldsymbol{\rho}}^j = \boldsymbol{b}^j, \tag{7}$$

with sensing matrix

$$\mathcal{A}^j = \begin{bmatrix} e^{\imath 2\frac{\omega_1}{c} r_1^j} & e^{\imath 2\frac{\omega_1}{c} r_2^j} & \ldots & e^{\imath 2\frac{\omega_1}{c} r_Q^j} \\ e^{\imath 2\frac{\omega_2}{c} r_1^j} & e^{\imath 2\frac{\omega_2}{c} r_2^j} & \ldots & e^{\imath 2\frac{\omega_2}{c} r_Q^j} \\ \vdots & & & \vdots \\ e^{\imath 2\frac{\omega_S}{c} r_1^j} & e^{\imath 2\frac{\omega_S}{c} r_2^j} & \ldots & e^{\imath 2\frac{\omega_S}{c} r_Q^j} \end{bmatrix}. \tag{8}$$

The superscript j is used to stress that (7) uses data recovered at location $\boldsymbol{x}_j$, which according to (5) has components

$$b_l^j = P(\boldsymbol{x}_j, \omega_l) e^{\imath\theta_j}, \quad l = 1, \ldots, S. \tag{9}$$

If the reflectivity vector $\tilde{\boldsymbol{\rho}}^j$ is sparse and the data are noiseless, the exact solution to (7) can be found by using ℓ_1-optimization algorithms under some conditions on the matrix $\mathcal{A}^j$ [3], [2], [4], [1].

The matrix $\mathcal{A}^j$ defined in (8) depends on the radii r_i^j, $i = 1, \ldots, Q$ which are computed in the following way. Given an IW of interest containing the discretization points $\boldsymbol{y}_k$, $k = 1, \ldots, K$ we compute the distances from all points $\boldsymbol{y}_k$ to the receiver location $\boldsymbol{x}_j$,

$$R_k^j = |\boldsymbol{y}_k - \boldsymbol{x}_j|. \tag{10}$$

These form the components of a vector in $\mathbb{R}^K$. We then sort the components of this vector in ascending order and keep only these entries that appear with multiplicity larger than one. More precisely, in practice we only keep the entries that differ from each other by at least a level ϵ. The value of ϵ should be small enough so that we do not disregard many components since that would affect the accuracy of the reconstruction but ϵ cannot be zero because we do not want the columns of $\mathcal{A}^j$ to be parallel. Assuming the R_k^j are ordered then this can be done as follows,

$$\begin{array}{l} \text{set } i = 1 \text{ and } r_i^j = R_i^j \\ \text{for k=2 to K} \\ \quad \text{if } |R_k^j - R_{k-1}^j| > \epsilon \\ \quad\quad \text{set } i = i + 1 \text{ and } r_i^j = R_k^j \\ \quad \text{end} \\ \text{end} \end{array} \tag{11}$$

This process generates the radii r_i^j, $i = 1, \ldots, Q$ with $Q \leq K$ which depend on the receiver location $j = 1, \ldots, N$.

Once the solution vector $\tilde{\boldsymbol{\rho}}^j$ has been found, we compute the total reflectivity within the IW, which is obtained by summing all the components of the vector $\tilde{\boldsymbol{\rho}}^j$, i.e.,

$$\sum_{q=1}^{Q} \tilde{\rho}_q^j \approx e^{\imath\theta_j} \frac{1}{h_c} \int_{IW} \boldsymbol{\rho}_0 d\vec{\mathbf{y}}, \tag{12}$$

with h_c a constant that depends on the discretization. The key point here is that for all receiver positions we can compute an approximation to the total reflectivity up to unknown phase factors $e^{\imath\theta_j}$, $j = 1, \ldots, N$. Thus, we can refer all the recovered quantities (9) to a same global phase with no meaning for imaging purposes. Indeed, let us define the quantities

$$c_j = \frac{\sum_{q=1}^{Q} \tilde{\rho}_q^j}{\sum_{q=1}^{Q} \tilde{\rho}_q^1} \overset{(12)}{=} e^{\imath(\theta_j - \theta_1)}, \ j = 1, \ldots, N, \tag{13}$$

by dividing the total reflectivities associated to every locations $\boldsymbol{x}_j$ by the total reflectivity obtained from the measurements recorded at $\boldsymbol{x}_1$. The choice of $j = 1$ in the denominator in (13) is, of course, arbitrary. With this choice, $c_1 = 1$. Then, by multiplying the recovered data (9) by $\overline{c_j}$ we get

$$\overline{c_j} b_l^j = P(\boldsymbol{x}_j, \omega_l) e^{\imath\theta_1}, \ \forall\, j = 2, \ldots, N \text{ and } l = 1, \ldots, S, \tag{14}$$

which define the holographic data

$$\begin{array}{ll} P^h(\boldsymbol{x}_1, \omega_l) & = b_l^1, \ \forall\, l = 1, \ldots, S. \\ P^h(\boldsymbol{x}_j, \omega_l) & = \overline{c_j} b_l^j, \ \forall\, j = 2, \ldots, N \text{ and } l = 1, \ldots, S. \end{array} \tag{15}$$

The phases in (15) are now coherent over different receiver positions and frequencies! Thus, the unknown reflectivity $\boldsymbol{\rho}$ can be reconstructed as if data with phases were recorded.

We want to emphasize that the proposed methodology allows one to produce holographic data from intensity measurements. This is of considerable importance since: i) Intensity data are much easier to obtain and can be performed with less expensive equipement (sensors) than holographic measurements. ii) Holographic data contain coherent phase information and allow us to obtain depth resolved reconstructions, iii)The proposed methodology does not need any prior information about the sought reflectivity. We compare next the performance of different imaging methods using (15) as data.

III. Full phase synthetic aperture imaging methods

Once the holographic data P^h are obtained, the unknown reflectivity can be reconstructed with any imaging method as

if the data with phases were recorded with a synthetic array aperture. Here we show results obtained with the frequently used Kirchhoff migration (KM) imaging method and the ℓ_1-optimization approach.

KM is a direct imaging method which can be written as

$$\rho^{KM}(\boldsymbol{y}_k) = \sum_{j=1}^{N}\sum_{l=1}^{S} e^{-\imath 2\frac{\omega_l}{c}|\boldsymbol{x}_j-\boldsymbol{y}_k|} P^h(\boldsymbol{x}_j,\omega_l), \qquad (16)$$

where $|\boldsymbol{x}_j - \boldsymbol{y}_k|$ is the distance between the measurement location $\boldsymbol{x}_j$ to the search point $\boldsymbol{y}_k$ in the imaging window IW. The image $\boldsymbol{\rho}^{KM} = [\rho^{KM}(\boldsymbol{y}_1), \rho^{KM}(\boldsymbol{y}_2)\ldots, \rho^{KM}(\boldsymbol{y}_K)]$ is an approximation to the unknown reflectivity vector $\boldsymbol{\rho}$.

We also find the reflectivity by promoting a sparse solution to the system

$$\mathcal{A}\boldsymbol{\rho} = \boldsymbol{b}\,, \qquad (17)$$

where $\boldsymbol{\rho} \in \mathbb{C}^K$ is the sought reflectivity vector,

$$\mathcal{A} = \begin{bmatrix} e^{\imath 2\frac{\omega_1}{c}|\boldsymbol{x}_1-\boldsymbol{y}_1|} & e^{\imath 2\frac{\omega_1}{c}|\boldsymbol{x}_1-\boldsymbol{y}_2|} & \ldots & e^{\imath 2\frac{\omega_1}{c}|\boldsymbol{x}_1-\boldsymbol{y}_K|} \\ e^{\imath 2\frac{\omega_1}{c}|\boldsymbol{x}_2-\boldsymbol{y}_1|} & e^{\imath 2\frac{\omega_1}{c}|\boldsymbol{x}_2-\boldsymbol{y}_2|} & \ldots & e^{\imath 2\frac{\omega_1}{c}|\boldsymbol{x}_2-\boldsymbol{y}_K|} \\ \vdots & \vdots & & \vdots \\ e^{\imath 2\frac{\omega_1}{c}|\boldsymbol{x}_N-\boldsymbol{y}_1|} & e^{\imath 2\frac{\omega_1}{c}|\boldsymbol{x}_N-\boldsymbol{y}_2|} & \ldots & e^{\imath 2\frac{\omega_1}{c}|\boldsymbol{x}_N-\boldsymbol{y}_K|} \\ e^{\imath 2\frac{\omega_2}{c}|\boldsymbol{x}_1-\boldsymbol{y}_1|} & e^{\imath 2\frac{\omega_2}{c}|\boldsymbol{x}_1-\boldsymbol{y}_2|} & \ldots & e^{\imath 2\frac{\omega_2}{c}|\boldsymbol{x}_1-\boldsymbol{y}_K|} \\ \vdots & \vdots & & \vdots \\ e^{\imath 2\frac{\omega_S}{c}|\boldsymbol{x}_N-\boldsymbol{y}_1|} & e^{\imath 2\frac{\omega_S}{c}|\boldsymbol{x}_N-\boldsymbol{y}_2|} & \ldots & e^{\imath 2\frac{\omega_S}{c}|\boldsymbol{x}_N-\boldsymbol{y}_K|} \end{bmatrix} \qquad (18)$$

is the model matrix, and $\boldsymbol{b} \in \mathbb{C}^{N\cdot S}$ is the recovered data vector whose components are

$$b_i = b_{(l-1)N+j} = P^h(\boldsymbol{x}_j,\omega_l),\ j = 1,\ldots,N, l = 1,\ldots,S. \qquad (19)$$

We note that the KM solution (16) can also be written as $\boldsymbol{\rho}^{KM} = \mathcal{A}^*\boldsymbol{b}$, where $\mathcal{A}^*$ is the complex conjugate transpose of $\mathcal{A}$.

To find the sparsest solution to the system (17), we solve the ℓ_1 optimization problem

$$\min \|\boldsymbol{\rho}\|_{\ell_1} \quad \text{subject to} \quad \mathcal{A}\boldsymbol{\rho} = \boldsymbol{b} \qquad (20)$$

using the algorithm GelMa described in Algorithm 1. This algorithm involves matrix-vector multiplications followed by a shrinkage-thresholding step defined by the operator

$$\eta_\tau(y_i) = \text{sign}(y_i)\max\{0, |y_i| - \tau\}.$$

In the noiseless case, it converges to the exact solution independently of the value of the regularization parameter τ [13]. It is a semi-implicit version of the primal-dual method [5].

Algorithm 1 GelMa for solving (20)

Require: Set $\boldsymbol{y} = \boldsymbol{0}$, $\boldsymbol{z} = \boldsymbol{0}$. Pick the step size β, and a regularization parameter τ.
repeat
Compute the residual $\boldsymbol{r} = \boldsymbol{b} - \mathcal{A}\boldsymbol{y}$
$\boldsymbol{y} \Leftarrow \eta_{\tau\beta}(\boldsymbol{y} + \beta\mathcal{A}^*(\boldsymbol{z} + \boldsymbol{r}))$
$\boldsymbol{z} \Leftarrow \boldsymbol{z} + \beta\boldsymbol{r}$
until Convergence

IV. Numerical simulations

We consider a high frequency microwave scanning regime with central frequency $f_0 = 50$GHz which corresponds to $\lambda_0 = 6$mm. We make measurements for $S = 41$ equispaced frequencies covering a total bandwidth of 10GHz using a single transmitter/receiver that is moving along a linear trajectory. The synthetic aperture is $a = 20$cm, and the distance from its center to the center of the IW is $L = 1$m; see Figure 3. We assume that the medium between the synthetic array and the IW is homogeneous. The size of the IW is $48\text{cm} \times 48\text{cm}$, and the pixel size is $6\text{mm} \times 6\text{mm}$. The measurements are gathered at $N = 41$ equispaced locations. These parameters are typical in microwave scanning technology [10].

We assume that the total power can be measured for a set of pulses of the form $cos(\omega_l t)\exp(-t^2/(2\sigma_t)^2)$, where ω_l is one of the targeted measurement frequencies and σ_t is the pulsewidth that is inversely proportional to the available bandwidth, B. As discussed in Appendix A to retrieve the phases for S frequencies $\omega_l, l = 1,\ldots,S$ we need to measure the total power for $3S-2$ illuminations. Since we measure total power, a simple strategy would be to use a sufficient delay between successive illuminations so that the corresponding echoes are non-overlapping. Given an illumination at time 0 an estimate for the starting time for the scattered signal is $\frac{2L}{c}$ while its duration is of the order $\frac{2\,\text{IW size}}{c}$. Thus as estimate of the acquisition time per location is $(3S-2)\left(\frac{1}{2B} + \frac{2\,\text{IW size}}{c} + \frac{2L}{c}\right)$. For the specific parameters used in the simulations this is $(3S-2)10\text{ns} = 1.2\mu\text{s}$.

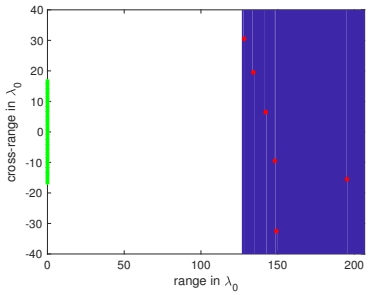

Fig. 3. The setup used in the numerical simulations. A single transmit/receive element is moving on a linear trajectory (green stars) and measures the intensity reflected from the scatterers (red disks). The blue area is the imaging window IW.

We add to the data mean zero uncorrelated noise corresponding to SNR = 10dB. Then we assume that only the amplitude of the reflected field can be measured and following the methodology described in Section II we recover from these phaseless data, the holographic data P^h (see (15)) which have phases that are coherent over frequency and measurement locations. In our numerical examples we used $\epsilon = 0.001\mu\text{m}$ in (11). Note that ϵ has units of length and is small with respect to the wavelength and the pixel size so that neglecting distances that differ less than ϵ does not affect the accuracy of the recovered phases. The recovered data P^h are then used for imaging the unknown reflectivity and the results are shown in Figure 4. The top row of Figure 4 shows the distribution

of targets we seek to find. The bottom left panel is the KM image, and the right panel is the image obtained with ℓ_1-optimization. As expected, KM shows resolution $\lambda_0 L/a$ in the cross-range direction and c/B in the range direction, which for our imaging setup corresponds to a resolution of $5\lambda_0$ in both directions. On the other hand, the image obtained with ℓ_1-optimization is almost exact.

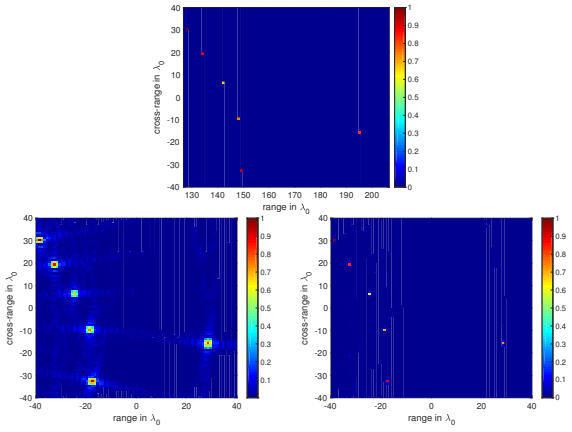

Fig. 4. Single transmitter/receiver multifrequency data recovered from intensity measurements with SNR $=$ 10dB. Imaging with KM as defined in (16) (left) and $\boldsymbol{\rho}^{\ell_1}$ computed using GelMa to solve (20) (right). On the top row the true reflectivity is plotted. In all images we plot the amplitude of the complex valued reflectivity $|\boldsymbol{\rho}|$.

To show the effectiveness of the method proposed here when phases are not recorded, we consider next the same imaging configuration but assume that the scatterers are displaced with respect to the grid points of the IW. Note that an error in the grid will affect the phase recovery as well as the actual image reconstruction. This is because the distance to the grid points R_k^j (see (10)) is used in the definition of the radii r_i^j in (8) and in the model matrix $\mathcal{A}$ (see (18)).

In Figure 5 we show results for scatterers that are displaced by $\lambda/8 = 0.75$mm (top row) and by $\lambda/2 = 3$mm (bottom row) with respect to the grid points in range and cross-range directions. The reconstructions do deteriorate as the displacement with respect to the grid increases but remain very satisfactory even for the largest possible displacement value of half the grid size (see bottom row plots in Figure 5). Last we also add to the data corresponding to the displacement $\lambda/2 = 3$mm mean zero uncorrelated noise corresponding to SNR $=$ 0dB. The results shown in Figure 6 are of very high quality and illustrate the robustness of the proposed methodology both to additive measurement type of noise as well as off-grid displacement errors.

V. Summary and Conclusions

We have introduced an approach to synthetic aperture imaging with intensity-only measurements by exploiting illumination diversity. The images have the same quality as when there is full phase information available. There are two stages in our approach. First we recover signal crosscorrelations over pairs of frequencies at each measurement location $\boldsymbol{x}_j$ using

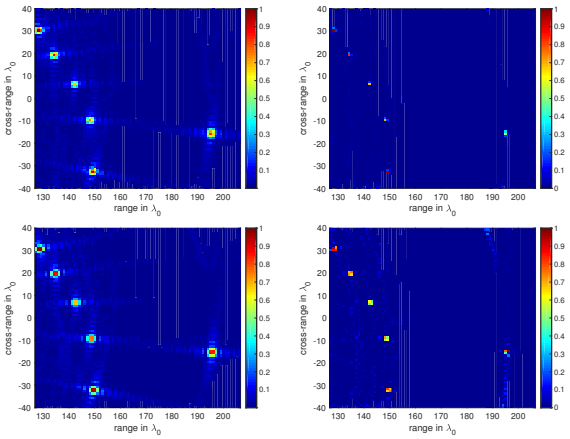

Fig. 5. Single transmitter/receiver multifrequency data recovered from intensity measurements. No additive noise is added to the data. Imaging with KM as defined in (16) (left) and $\boldsymbol{\rho}^{\ell_1}$ computed using GelMa to solve (20) (right). The scatterers are displaced by $\lambda/8 = 0.75$mm (top row) and by $\lambda/2 = 3$mm with respect to the grid points in range and cross-range directions. In all images we plot the amplitude of the complex valued reflectivity $|\boldsymbol{\rho}|$.

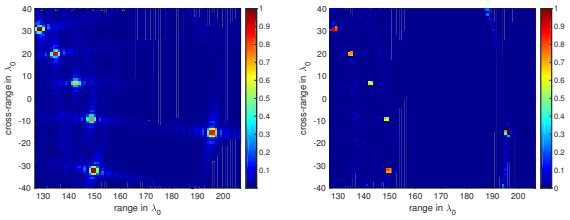

Fig. 6. Single transmitter/receiver multifrequency data recovered from intensity measurements with SNR $=$ 0dB. Imaging with KM as defined in (16) (left) and $\boldsymbol{\rho}^{\ell_1}$ computed using GelMa to solve (20) (right). The scatterers are displaced by $\lambda/2 = 3$mm with respect to the grid points in range and cross-range directions. In all images we plot the amplitude of the complex valued reflectivity $|\boldsymbol{\rho}|$.

intensity only measurements and the polarization identity. This way phases are recovered up to a location dependent factor $e^{\imath\theta_j}$. In the second stage, which is the main contribution of this paper, we introduce an algorithm (see Section II-B) that recovers the missing phases up to a single global factor $e^{\imath\theta_1}$. We can then image with any method that uses full phase data. We explore this approach with broadband SAR in the 50GHz regime in an imaging setup that is used in security scanning equipment.

Appendix A
Illumination Strategies

We discuss here an illumination strategy for recovering the phase cross-correlations from intensity measurements at different frequencies using a single transmit/receive element. The same illumination protocol can be used whether the intensities or the total power is measured. In this protocol at each transmit/receive location we need to record measurements corresponding to $3S - 2$ illuminations. We explain next the proposed protocol.

We want to recover the cross-correlation matrix

$$[\boldsymbol{M}^j]_{ll'} \equiv m^j_{ll'} = \overline{P(\boldsymbol{x}_j,\omega_l)}P(\boldsymbol{x}_j,\omega_{l'}), \quad l,l' = 1,\ldots,S\ , \tag{21}$$

using diversity of illuminations and the polarization identities

$$\mathrm{Re}(m^j_{ll'}) = \frac{1}{2}\left(|\mathbf{P}^j\cdot\boldsymbol{e}_{l+l'}|^2 - |\mathbf{P}^j\cdot\boldsymbol{e}_l|^2 - |\mathbf{P}^j\cdot\boldsymbol{e}_{l'}|^2\right) \tag{22}$$

$$\mathrm{Im}(m^j_{ll'}) = \frac{1}{2}\left(|\mathbf{P}^j\cdot\boldsymbol{e}_{l-\imath l'}|^2 - |\mathbf{P}^j\cdot\boldsymbol{e}_l|^2 - |\mathbf{P}^j\boldsymbol{e}_{l'}|^2\right). \tag{23}$$

When intensities are recorded then this means that all the quantities $|\cdot|^2$ in the right hand side of (22) and (23) can be measured. When the total power is recorded, given an illumination $\boldsymbol{f}\in\mathbb{C}^S$ the corresponding measurement is

$$\begin{aligned}|\boldsymbol{P}^j\cdot\boldsymbol{f}|^2 &= |\sum_{l=1}^S P(\boldsymbol{x}_j,\omega_l)f_l|^2\\ &= \sum_{l,l'=1}^S \overline{f_l}\overline{P(\boldsymbol{x}_j,\omega_l)}P(\boldsymbol{x}_j,\omega_{l'})f_{l'}\\ &= \sum_{l,l'=1}^S \overline{f_l}m^j_{ll'}f_{l'} = \boldsymbol{f}^*\boldsymbol{M}^j\boldsymbol{f}.\end{aligned}$$

Therefore, again we can measure all the quantities in the right hand side of the polarization identities. Remarking that

$$m^j_{ll'} = \frac{m^j_{l1}m^j_{1l'}}{m^j_{11}}\ ,$$

we deduce that we only need to compute the phase cross-correlations $m^j_{l1}m^j_{1l'}$ which can be obtained from the polarization identities (22)-(23) provided $3S-2$ measurements. Indeed we can determine m^j_{l1}, for $l=2,\ldots,S$ using illuminations $\boldsymbol{e}_l$, $\boldsymbol{e}_{l+1}$ and $\boldsymbol{e}_{l-\imath 1}$ and we also need to measure m^j_{11}.

ACKNOWLEDGMENTS

The work of M. Moscoso was partially supported by Spanish grant MICINN FIS2016-77892-R. The work of A.Novikov was partially supported by NSF grant NSF DMS-1813943. The work of C. Tsogka was partially supported by AFOSR FA9550-17-1-0238.

REFERENCES

[1] L. BORCEA AND I. KOCYIGIT, *Resolution analysis of imaging with ℓ_1 optimization*, SIAM J. Imaging Sci. 8 (2015), pp. 3015–3050.

[2] E.J CANDÈS. J.K. ROMBERG, AND T. TAO, *Stable signal recovery from incomplete and inaccurate information,* Communications on Pure and Applied Mathematics 59 (2006), pp. 1207–33.

[3] D. DONOHO AND M. ELAD, *Optimally sparse representation in general (nonorthogonal) dictionaries via ℓ_1 minimization*, Proceedings of the National Academy of Sciences 100 (2003), pp. 2197–2202.

[4] A. FANNJIANG AND W. LIAO, *Coherence pattern-guided compressive sensing with unresolved grids,* SIAM J. Imaging Sci. 5 (2012), pp. 179–202.

[5] A. CHAMBOLLE AND T. POCK, *A first-order primal-dual algorithm for convex problems with applications to imaging,* Journal of Mathematical Imaging and Vision (2011).

[6] S. CONSTANZO, G. D, MASSA, AND M. D. MIGLIORE, *A novel hybrid approach for far-field characterization from near-field amplitude- only measurements on arbitrary scanning surfaces,* IEEE Trans. Antennas Propag. 53 (20015), pp. 1866–1874.

[7] J.R. FIENUP, *Phase retrieval algorithms: a comparison,* Applied Optics 21 (1982), pp. 2758–2768.

[8] G. JUNKIN, *Planar near-field phase retrieval using GPUs for accurate THz far-field prediction,* IEEE Trans. Antennas Propag. 61 (2013), pp. 1763–1776.

[9] J. LAVIADA,Y. ALVAREZ-LOPEZ, C. GARCIA-GONZALEZ, C. VASQUEZ-ANTUNA, S. VER-HOYE, M. FERNADEZ-GARCIA, G. HOTOPAN, R. CAMBLOR AND F. LAS-HERAS, *A novel phaseless frequency scanning based on indirect holography,* J. Electromagn. Waves Appl., 27:4 (2013), pp. 275–296.

[10] J. LAVIADA, A. ARBOLEYA-ARBOLEYA, Y. ALVAREZ-LOPEZ, C. GARCIA-GONZALEZ AND F. LAS-HERAS, *Phaseless synthetic aperture radar with efficient sampling for broadband near-field imaging: Theory and validation,* IEEE Trans. Antennas Propag., 63:2 (2015), pp. 573–584.

[11] E. N. LEITH AND J. UPATNIEKS, *Reconstructed waveforms and communication theory,* J. Opt. Soc. Amer., 52 (1962), pp. 1123–1128.

[12] A. LEHTO, J. TUOVINEN, O. BORIC AND A. RAISANEN, *Accurate millimeter wave antenna phase pattern measurements using the differential phase method with three power meters,* IEEE Transactions on Antennas and Propagation 40 (1992), pp. 851-853.

[13] M. MOSCOSO, A. NOVIKOV, G. PAPANICOLAOU AND L. RYZHIK, *A differential equations approach to l1-minimization with applications to array imaging,* Inverse Problems 28 (2012).

[14] M. MOSCOSO, A. NOVIKOV AND G. PAPANICOLAOU, *Coherent imaging without phases,* SIAM J. Imaging Sci. 9 (2016), pp. 1689–1707.

[15] M. MOSCOSO, A. NOVIKOV, G. PAPANICOLAOU AND C. TSOGKA, *Multifrequency interferometric imaging with intensity-only measurements,* SIAM J. Imaging Sci. 10 (2017), pp. 1005–1032.

[16] A. NOVIKOV, M. MOSCOSO AND G. PAPANICOLAOU, *Illumination strategies for intensity-only imaging,* SIAM J. Imaging Sci., 8 (2015), pp. 1547–1573.

[17] W.-J. ZHAO, B.-F. WANG, E.-X. LIU, H.-B. PARK, H. H. PARK, E. SONG, AND E.-P. LI, *An effective and efficient approach for radiated emission prediction based on amplitude-only near-field measurements,* IEEE Trans. Electromagn. Compat. 54 (2012) pp. 1186–1189.